China Ocean Eng., Vol. 29, No. 1, pp. 1 – 16

DOI 10.1007/s13344-015-0001-7, ISSN 0890-5487

Focused Wave Properties Based on A High Order Spectral Method with A Non-Periodic Boundary*

LI Jin-xuan (李金宣)[1] and LIU Shu-xue (柳淑学)

State Key Laboratory of Coastal and Offshore Engineering, *Dalian University of Technology*, *Dalian 116024*, *China*

(Received 26 February 2014; accepted 10 April 2014)

ABSTRACT

In this paper, a numerical model is developed based on the High Order Spectral (HOS) method with a non-periodic boundary. A wave maker boundary condition is introduced to simulate wave generation at the incident boundary in the HOS method. Based on the numerical model, the effects of wave parameters, such as the assumed focused amplitude, the central frequency, the frequency bandwidth, the wave amplitude distribution and the directional spreading on the surface elevation of the focused wave, the maximum generated wave crest, and the shifting of the focusing point, are numerically investigated. Especially, the effects of the wave directionality on the focused wave properties are emphasized. The numerical results show that the shifting of the focusing point and the maximum crest of the wave group are dependent on the amplitude of the focused wave, the central frequency, and the wave amplitude distribution type. The wave directionality has a definite effect on multidirectional focused waves. Generally, it can even out the difference between the simulated wave amplitude and the amplitude expected from theory and reduce the shifting of the focusing points, implying that the higher order interaction has an influence on wave focusing, especially for 2D wave. In 3D wave groups, a broader directional spreading weakens the higher nonlinear interactions.

Key words: *focused wave*; *high order spectral method*; *numerical model*

1. Introduction

Offshore structures are constantly exposed to violent wave impacts. The ambient wave conditions and their properties must be determined before the design of ocean structures can proceed. Accurate estimation and understanding of severe extreme events are essential for human safety and for cost-effective design.

Several mechanisms have been proposed to explain the generation of extreme waves, such as wave focusing, wave–current interaction, and modulation instability (Kharif and Pelinovsky, 2003). Wave focusing is the most important of these mechanisms. Many researchers have paid considerable attention to the study of wave focusing, with the aim of understanding the physical mechanisms by which large waves are created (Rapp and Melville, 1990; Baldock *et al*., 1996; Li *et al*., 2008). But most of these studies were focused on two-dimensional waves. However, waves in the ocean are multidirectional. Focused waves are generated not only by the focusing of waves with different frequencies, but also by that of waves with different directions. The wave directionality has a definite

* This project was financially supported by the National Natural Science Foundation of China (Grant Nos. 51309050 and 51221961), and the National Basic Research Program of China (973 Program, Grant Nos. 2013CB036101 and 2011CB013703).

1 Corresponding author. Email: lijx@dlut.edu.cn

effect on their propagation. She *et al*. (1994) examined the effects of wave directionality on breaking waves and on their kinematics by investigating two simple cases of a wave field: one formed from waves with a single frequency with a uniform angular spread, and one formed from waves with multiple frequencies where the waves of each frequency had a specified angular spreading function. Their results showed that the height of the incipient breaking wave, the crest elevation, the crest front steepness, and the vertical asymmetry factor depended strongly on the angular spread. Johannessen and Swan (2001) demonstrated clearly the need to incorporate the directionality of a wave field if extreme ocean waves were to be accurately modelled and their physical characteristics explained. Wu and Nepf (2002) examined the effects of wave directionality on the criterion for waves breaking. Their results showed that the wave directionality and the spectral shape can affect the local wave shape parameters at the onset of wave breaking. However, the properties of focused waves, especially in the case of multidirectional waves, are not yet fully understood, owing to the complexity of the problem.

In addition to experimental methods, numerical methods are major methods for the study of wave propagation. Several different models can be used to simulate the focusing of waves. For instance, Brandini and Grilli (2001) carried out a three-dimensional numerical study of spatial wave focusing using the boundary element model with an Eulerian–Lagrangian flow representation. Dommermuth and Yue (1987) and West *et al*. (1987) developed the High Order Spectral (HOS) method to solve the derivative terms by Fast Fourier Transform (FFT) method. Compared with other methods, the spectral method has the properties of fast convergence and low computational cost. The original method permits the fully nonlinear simulation of the evolution of gravity waves within periodic unbounded three-dimensional domain by giving the initial surface elevation and velocity potential. Bonnefoy *et al*. (2004) extended the method to simulate the generation and propagation of focused waves by introducing the concept of an additional potential that satisfied a non-homogeneous boundary condition. Bonnefoy *et al*. (2009) and Ducrozet *et al*. (2012) further improved the wave maker boundary modelling up to the second- and third-order, respectively.

In this paper, a numerical method is developed based on the HOS formulation of Dommermuth and Yue (1987) for non-periodic boundary. A wave maker boundary condition is introduced to simulate the wave generation at the incident boundary in the HOS method. Then, the method for the generation of multidirectional focused waves is described. The effects of the wave parameters, such as the assumed focused amplitude, the central frequency, the frequency bandwidth, the wave amplitude distribution and the directional spreading on the surface elevation of the focused wave, the maximum generated wave crest, and the shifting of the focusing point, are numerically investigated.

2. Numerical Model

2.1 Governing Equations

It is assumed that the fluid is incompressible and inviscid, and the flow is irrotational. The velocity potential $\Phi(x, y, z, t)$ in the fluid domain satisfies Laplace's equation,

$$\nabla^2\Phi(x,y,z,t)=0\,. \tag{1}$$

Following Zakharov (1968), the fully nonlinear free surface boundary conditions can be expressed

in terms of the velocity potential at the water surface as:

$$\frac{\partial \eta}{\partial t}=\left(1+\left|\nabla_x \eta\right|^2\right)\frac{\partial \Phi}{\partial z}-\nabla_x \Phi^s \nabla_x \eta\,,\quad z=\eta\,; \tag{2}$$

$$\frac{\partial \Phi^s}{\partial t}=-g\eta-\frac{1}{2}\left|\nabla_x \Phi^s\right|^2+\frac{1}{2}\left(1+\left|\nabla_x \eta\right|^2\right)\left(\frac{\partial \Phi}{\partial z}\right)^2,\quad z=\eta\,, \tag{3}$$

where $\Phi^s(x,y,t)=\Phi(x,y,\eta,t)$ is the velocity potential on the water surface $z=\eta$, and $\nabla_x=(\partial/\partial x,\partial/\partial y)$. On the fixed boundaries (the bottom, side, and end walls of the tank), the conditions can be written simply as:

$$\nabla\Phi\cdot\boldsymbol{n}=0\,, \tag{4}$$

where $\boldsymbol{n}$ is a vector normal to the boundary considered.

2.2 Non-Periodic Boundary/Wave Maker Boundary

For a typical wave basin, one boundary of the domain will correspond to a wave maker. So if the wave maker boundary is assigned to the left of the wave basin, as shown in Fig. 1, the corresponding boundary condition can be written as:

$$\frac{\partial \Phi}{\partial x}=\frac{\partial X(y,t)}{\partial t}=U(y,t)\quad \text{on}\quad x=0\,, \tag{5}$$

where $X(t)$ is the displacement of the wave maker board and $U(t)$ is the horizontal velocity of the wave maker.

According to linear wave maker theory (Dean and Dalrymple, 1984), the velocity of the incident wave can be calculated from the following equation:

$$U(y,t)=\frac{\omega}{T(\omega,\theta)}\eta\,, \tag{6}$$

where ω is the wave frequency, η is the expected wave surface, and θ is the wave direction. $T(\omega, \theta)$ is the transfer function for a piston-type wave maker and can be calculated from the following equation for three-dimensional waves:

$$T(\omega,\theta)=\frac{2\left[\cosh(2kh)-1\right]}{\left[2kh+\sinh(2kh)\right]\cos\theta}\,, \tag{7}$$

where k is the wave number and h is the water depth.

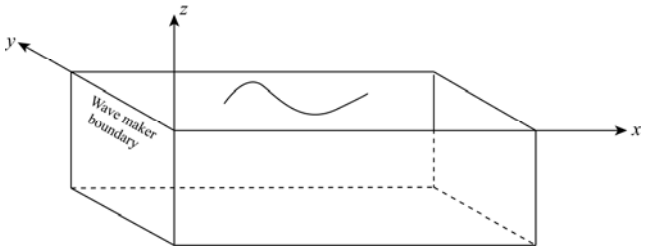

Fig. 1. Sketch of a wave basin and its coordinate system.

2.3 Numerical Procedure

In order to solve this non-homogeneous problem, following Agnon and Bingham (1999) and Bonnefoy *et al*. (2004), the velocity potential can be split into two parts, i.e.,

$$\Phi = \Phi_{\mathrm{f}} + \Phi_{\mathrm{w}}\,, \tag{8}$$

where Φ_{f} is unknown and satisfies free wave surface boundary conditions, and the prescribed non-periodic component Φ_{w} satisfies the wave maker boundary condition Eq. (5) and other lateral boundary conditions. So Eqs. (2) and (3) can be rewritten as follows:

$$\frac{\partial \eta}{\partial t} = \left(1+\left|\nabla_x \eta\right|^2\right)\frac{\partial \Phi_{\mathrm{f}}}{\partial z} + \frac{\partial \Phi_{\mathrm{w}}}{\partial z} - \nabla_x(\Phi_{\mathrm{f}}^{\mathrm{s}} + \Phi_{\mathrm{w}})\cdot\nabla_x \eta\,,\quad z=\eta\,; \tag{9}$$

$$\begin{aligned}\frac{\partial \Phi_{\mathrm{f}}^{\mathrm{s}}}{\partial t} = {} & -g\eta - \frac{1}{2}\left|\nabla_x \Phi_{\mathrm{f}}^{\mathrm{s}}\right|^2 + \frac{1}{2}\left(1+\left|\nabla_x \eta\right|^2\right)\left(\frac{\partial \Phi_{\mathrm{f}}}{\partial z}\right)^2 \\ & - \nabla_x \Phi_{\mathrm{f}}^{\mathrm{s}}\cdot\nabla_x \Phi_{\mathrm{w}} - \frac{\partial \Phi_{\mathrm{w}}}{\partial t} - \frac{1}{2}\left|\nabla_x \Phi_{\mathrm{w}}\right|^2 - \frac{1}{2}\left(\frac{\partial \Phi_{\mathrm{w}}}{\partial z}\right)^2,\quad z=\eta.\end{aligned} \tag{10}$$

Therefore, determining Φ_{w} becomes the first key problem in establishing the numerical model using the HOS method. Several different expansions can be chosen for it. For example, Agnon and Bingham (1999) used polynomials in a two-dimensional wave tank simulation, whereas Bonnefoy *et al*. (2004) employed a spectral expansion in two-dimensional and three-dimensional wave tank simulations. Following Bonnefoy *et al*. (2004), to obtain an expression for the non-periodic component Φ_{w}, we extend the computational domain into three parts as shown in Fig. 2, in which the lower part is the real domain and the upper parts are mirror images of the lower part and the middle part is the transition region. The wave making condition can be expressed as:

$$\frac{\partial \Phi_{\mathrm{w}}}{\partial x} = \begin{cases} -\dfrac{\partial X(y,t)}{\partial t} & 2h \le z \le 3h \\ \dfrac{\partial X(y,t)}{\partial t}\cos\left(\dfrac{z}{2h}\pi\right) & 0 < z < 2h \\ \dfrac{\partial X(y,t)}{\partial t} & -h \le z \le 0 \end{cases} \tag{11}$$

In addition to Eq. (11), Φ_{w} also satisfies the following equations:

$$\nabla^2 \Phi_{\mathrm{w}}(x,y,z,t) = 0\,; \tag{12}$$

$$\frac{\partial \Phi_{\mathrm{w}}}{\partial x} = 0\,,\quad x = L_x\,; \tag{13}$$

$$\frac{\partial \Phi_{\mathrm{w}}}{\partial y} = 0\,,\quad y = 0\,,\ y = L_y\,; \tag{14}$$

$$\frac{\partial \Phi_{\mathrm{w}}}{\partial z} = 0\,,\quad z = -h\,,\ z = 3h\,. \tag{15}$$

The extension of the computational domain has been made in an anti-symmetric way with respect to $z = h$, as can be seen from Eq. (11) and therefore the potential is odd with respect to $z = h$.

By using the separation method of variables, the solution for Φ_{w} can be expressed as:

$$\Phi_{\mathrm{w}}(x,y,z,t) = \sum_{p=0}^{N_y}\sum_{q=0}^{N_z} A_{pq}(t)\frac{\cosh[k_{pq}(L_x - x)]}{\cosh(k_{pq}L_x)}\cos(k_p y)\cos[k_q(z+h)]\,, \tag{16}$$

where $A_{pq}(t)$ are the unknown component amplitudes to be determined according to the generated waves that are desired, $k_p = \dfrac{p\pi}{L_y}$, $k_q = \dfrac{(2q-1)\pi}{4h}$, and $k_{pq} = \sqrt{\left(\dfrac{p\pi}{L_y}\right)^2 + \left(\dfrac{(2q-1)\pi}{4h}\right)^2}$.

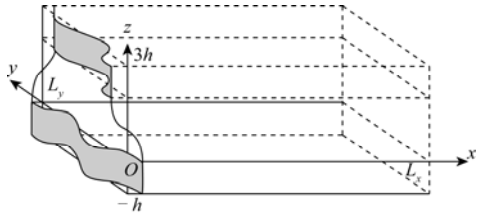

Fig. 2. Sketch of the extension of a wave basin.

So the space and time derivations of Φ_w can be easily derived from Eq. (16). From Eq. (11), we can obtain

$$\frac{\partial^2 \Phi_w}{\partial x \partial t} = \begin{cases} -\dfrac{\partial^2 X(y,\ t)}{\partial t^2} & 2h \le z \le 3h \\ \dfrac{\partial^2 X(y,\ t)}{\partial t^2}\cos\left(\dfrac{z}{2h}\pi\right) & 0 < z < 2h \\ \dfrac{\partial^2 X(y,\ t)}{\partial t^2} & -h \le z \le 0 \end{cases} \tag{17}$$

By substituting Eq. (16) into Eqs. (11) and (17), the coefficients $A_{pq}(t)$ and $A'_{pq}(t)$ can be solved.

The unknown component Φ_f satisfies the free-surface boundary conditions Eqs. (9) and (10) and the lateral boundary conditions Eq. (4). The component can be solved by the HOS method (Dommermuth and Yue, 1987).

The time integration of Eqs. (9) and (10) was performed by a fifth-order Runge–Kutta scheme in the present study. A 'sponge' layer, as proposed by Larsen and Dancy (1983), was used to absorb the incoming wave energy at the right-hand boundary of the wave basin. In the sponge layer, the velocity potential Φ and the surface elevation η are divided by $\mu(x, y)$ after each time step. The sponge layer can be written as:

$$\mu(x,y) = \begin{cases} \exp\left[\left(2^{\frac{d}{l\Delta d}} - 2^{\frac{d_z}{l\Delta d}}\right)\ln\alpha\right] & 0 \le d \le d_z \\ 1 & d_z \le d \end{cases} \tag{18}$$

where, d is the distance between grid point and boundary, Δd is grid spacing and d_z is the width of the sponge layer. The parameters l and α are constants, selected as $l = 5$ and $\alpha = 4.0$, respectively in this study.

3. General Description of the Generation of Focused Waves

According to the linear wave theory, the free water surface $\eta(x, y, t)$ for a three-dimensional sea can be represented by a double-summation model as:

$$\eta(x,y,t)=\sum_{i=1}^{N_f}\sum_{j=1}^{N_\theta}a_{ij}\cos\left(k_i x\cos\theta_j+k_i y\sin\theta_j-2\pi f_i t-\varphi_{ij}\right), \tag{19}$$

where a_{ij} is the amplitude of the component wave with the i-th frequency f_i and the j-th direction θ_j; k_i is the wave number; φ_{ij} is the phase of the wave component; N_f and N_θ are the numbers of the frequencies and directions, respectively. N_f =29 and N_θ=200 are used for investigation in this paper. The frequency f_i and the wave number k_i are related to each other by a linear dispersion equation as follows:

$$\omega_i^2=(2\pi f_i)^2=k_i g\tanh\left(k_i h\right), \tag{20}$$

where h is the water depth.

If the waves are assumed to be focused at a specified position (x_b, y_b) and time t_b, then the surface wave elevation can be written as (Liu and Hong, 2005):

$$\eta(x,y,t)=\sum_{i=1}^{N_f}\sum_{j=1}^{N_\theta}a_{ij}\cos[k_i(x-x_b)\cos\theta_j+k_i(y-y_b)\sin\theta_j-2\pi f_i(t-t_b)], \tag{21}$$

in which the amplitude of each wave component a_{ij} can be determined from the following equation:

$$a_{ij}=AS_a\left(f_i\right)G_a\left(\theta_j\right)\mathrm{d}f\mathrm{d}\theta, \tag{22}$$

where, df and dθ are the frequency and direction increments. A is the focused wave amplitude, and is equal to the sum of the amplitude of each component a_{ij}:

$$A=\sum_{i=1}^{N_f}\sum_{j=1}^{N_\theta}a_{ij}\ . \tag{23}$$

$G_a(\theta)$ is the directional spreading function, and the following form is used:

$$G_a\left(\theta_j\right)=\frac{\cos^{2s}\left(\theta_j/2\right)}{\sum_{j=1}^{N_\theta}\cos^{2s}\left(\theta_j/2\right)\mathrm{d}\theta}\qquad |\theta|<\theta_{\max} \tag{24}$$

where s is the parameter that describes the directional concentration, and θ_{max} is the maximum direction allowed by the spreading function.

In Eq. (22), $S_a(f)$ is the amplitude distribution. Three kinds of distributions are considered. The first is the constant wave amplitude (CWA) distribution. This means that the wave amplitude of each component wave in the same direction is constant. So $S_a(f_i)$ can be expressed as:

$$S_a\left(f_i\right)=\frac{1}{N_f\mathrm{d}f}\ . \tag{25}$$

The second kind of amplitude distribution is the constant wave steepness (CWS) distribution. In this case, the steepness of each component wave is assumed to be a constant. Then $S_a(f_i)$ can be derived from

$$S_a\left(f_i\right)=\frac{1}{k_i\sum_{n=1}^{N_f}\frac{1}{k_n}\mathrm{d}f}\ . \tag{26}$$

The third kind of amplitude distribution is the normalized JONSWAP distribution (NJS). In this case, $S_a(f_i)$ can be calculated from

$$S_{\mathrm{a}}(f_i)=\frac{S(f_i)}{\sum_{n=1}^{N_f}S(f_n)\mathrm{d}f}, \tag{27}$$

where $S(f)$ uses the general JONSWAP type spectrum (Goda, 1999) with the peak enhancement factor $\gamma=3.3$. To provide an intuitive understanding, a typical comparison of the three kinds of amplitude distributions is shown in Fig. 3.

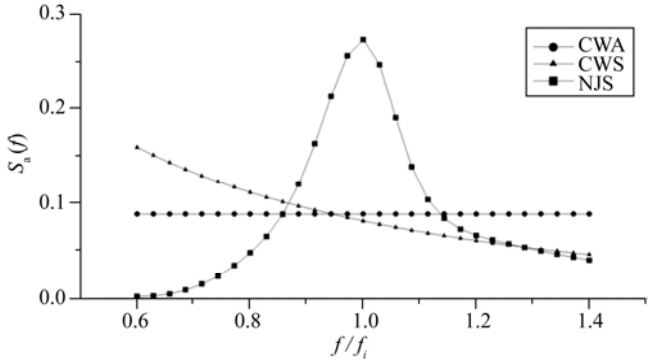

Fig. 3. Comparison of the three kinds of amplitude distributions.

The discrete frequencies f_i in Eq. (22) are uniformly spaced over the frequency band $[f_1, f_n]$. The frequency bandwidth Δf and the central frequency f_c are defined as:

$$\Delta f=f_n-f_1;\quad f_{\mathrm{c}}=\frac{1}{2}(f_1+f_n). \tag{28}$$

But as an exception, the peak period $T_p=1/f_c$ is used in the JONSWAP spectrum. In this paper, Δf is used to describe the frequency component distribution. However, form Fig. 3, it can be seen that the energy distributions are different for the three kinds of amplitude distributions. The energy of NJS distribution is more concentrated than those of the other two.

4. Verification of the Numerical Model

The first example is a comparison between the two-dimensional experimental focused wave data and numerical results. A focused wave experiment was conducted in a two-dimensional wave flume with A = 0.06 m, f=0.5–1.36 Hz, and f_c=0.83 Hz. The corresponding wave steepness k_cA was 0.18. The waves were assumed to be focused at a distance 11.4 m away from the wavemaker. The NJS amplitude distribution was used, and the water depth was 0.5 m (k_ch=1.54). The length of the numerical wave tank is 40 m. The numerical simulations were performed with N_x=401, N_z=101, and M=5. Fig. 4 presents the comparisons of the numerical and experimental time histories of the wave at the focusing point. The figure shows that the simulated focused wave surfaces agree well with the experimental data. However, the numerical and experimental values of the focused wave amplitude are larger than the assumed amplitude because of the nonlinear wave evolution.

The second example is based on directional focused waves. The numerical area was $L_x\times L_y$=20 m ×28 m, and the water depth was 0.3 m. The focusing amplitude was assumed to be 0.029 m, the

frequency range was 0.50–1.10 Hz, the central frequency f_c was 0.80 Hz, the steepness k_cA was 0.11 (where k_c is the wave number corresponding to the central frequency) and k_ch=1.0. The maximum direction θ_{max} was 60° and the directional spreading parameter s was equal to 0 (uniform distribution). The focusing time and point were 24.0 s and (8.0 m, 14.0 m), respectively. In the simulation, 201×281 modes were used on the free surface, 281×64 on the wave maker boundary, and order M=4. The time interval was 0.04 s. The total CPU time for 35.0 s duration simulation was around 7.0 h on a 2.9 GHz processor.

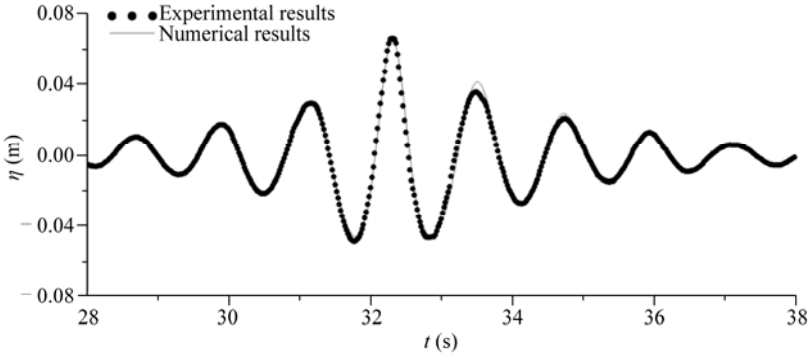

Fig. 4. Comparison between experimental data (solid line) and numerical results (dotted line) for two-dimensional focused waves for the case with A=0.06 m, f=0.5–1.36 Hz, and f_c=0.83 Hz.

Fig. 5 presents the typical surface elevations of three-dimensional focused waves at selected time. To provide an intuitive understanding, Fig. 5a shows the focusing of three-dimensional waves with a single frequency (i.e., with N_f=1 in Eq. (23)). From Fig. 5, we can observe the development of three-dimensional focused waves. As expected, the component waves with different frequencies and directions are focused at the focusing point. Before the focusing time, waves are generated by the wave maker and the wave crests become larger as the wave is focused. The waves are focused together near the assumed focusing point at the assumed focusing time. After the focusing point, the focused wave is dispersed. To show the accuracy of the numerically calculated directional focused waves, Fig. 6 shows a comparison of numerically calculated surface elevations and a second-order theoretical results (Sharma and Dean, 1981) at the focusing point. It can be seen that there is a perfect agreement between the theoretical and numerical results.

These examples demonstrate that the numerical model has the capability to simulate the wave generation and focusing, and can be used to numerically study the characteristics of focused waves.

5. Numerical Investigation of the Properties of Focused Waves

5.1 Two-Dimensional Focused Waves

In the two-dimensional cases, three different amplitude distributions, namely the CWS, CWA and NJS distribution, were used. For each case, the assumed focused wave amplitude varied in the range of 0.01–0.08 m, the frequency bandwidth Δf varied in the range of 0.46–0.86 Hz, and the central frequency f_c varied in the range of 0.63–0.93 Hz. In all cases, the maximum wave steepness k_cA was smaller than 0.25. The water depth was 0.5 m and the assumed focusing time and location were 30 s

and 12.3 m, respectively. The numerical wave tank is 40 m long. The numerical simulations were performed with following parameters N_x=401, N_z=100 and M=5.

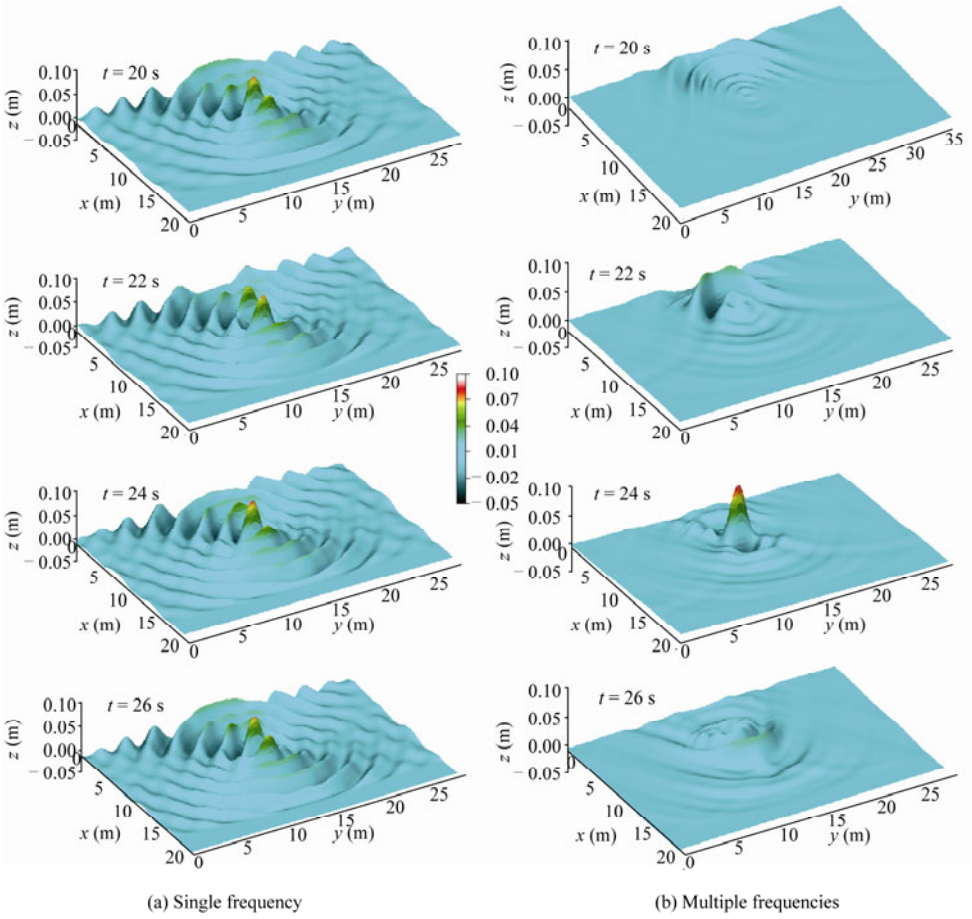

Fig. 5. Typical surface elevations of three-dimensional focused waves at selected time (A=0.029 m, k_cA=0.11, θ_{max}=60°).

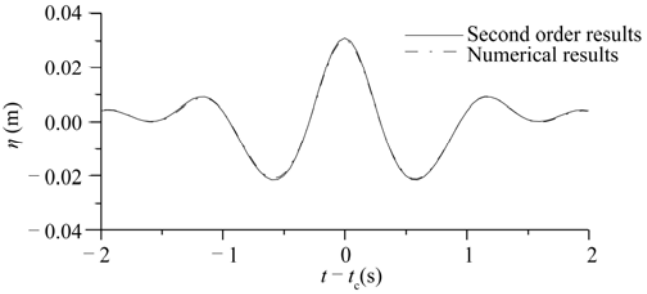

Fig. 6. Comparison between numerical results and a theoretical second order Stokes wave (A=0.029 m, f=0.50–1.10 Hz, k_cA=0.11, θ_{max}=60°).

During wave focusing process, wave properties (such as the shift of focusing point and the maximum crest) will change owing to the nonlinear interactions. The changes of wave properties reflect the strength of the nonlinear interaction. In general, the focusing point can be determined using

the principle that at that point, the wave troughs on either side of the largest wave crest should be of equal depth and the adjacent waves should be of similar amplitude (Baldock, 1994). For focused wave groups, the focusing point was not exactly at the position expected from linear theory because of the third-order nonlinear effects that modified the phase speed of wave components in the propagation of the wave packet. Fig. 7 shows the numerically calculated shift distance Δx of the focusing point for different wave parameters. Fig. 7a presents the effects of the amplitude of the focused wave on the shift for different amplitude distributions. This figure shows that the shift of the focusing point increases as the assumed focused amplitude increases. This is reasonable because the shift distance depends on $k_c A^2$ according to the third-order theory. Fig. 7b shows the variation of the shift of the focusing point with the frequency bandwidth. The shift becomes smaller as the frequency bandwidth increases. This means that the high order nonlinear becomes weaker when wave components distributions are wider. Fig. 7c shows the effect of the central frequency on the shift of the focal point. It can be seen that the shift of the focusing point increases linearly as the central frequency increases. The shift of the focusing point is also dependent on the wave amplitude distribution. This can be attributed to the more concentrated energy distribution with NJS distribution (see Fig. 3). As mentioned above, the shift of the focusing point is caused by strong nonlinear interactions between the wave components. The results imply that there are strong nonlinear interactions during wave focusing process, and the nonlinearity increases as the amplitude and central frequency increase (i.e. the wave steepness increases) and the frequency bandwidth decreases.

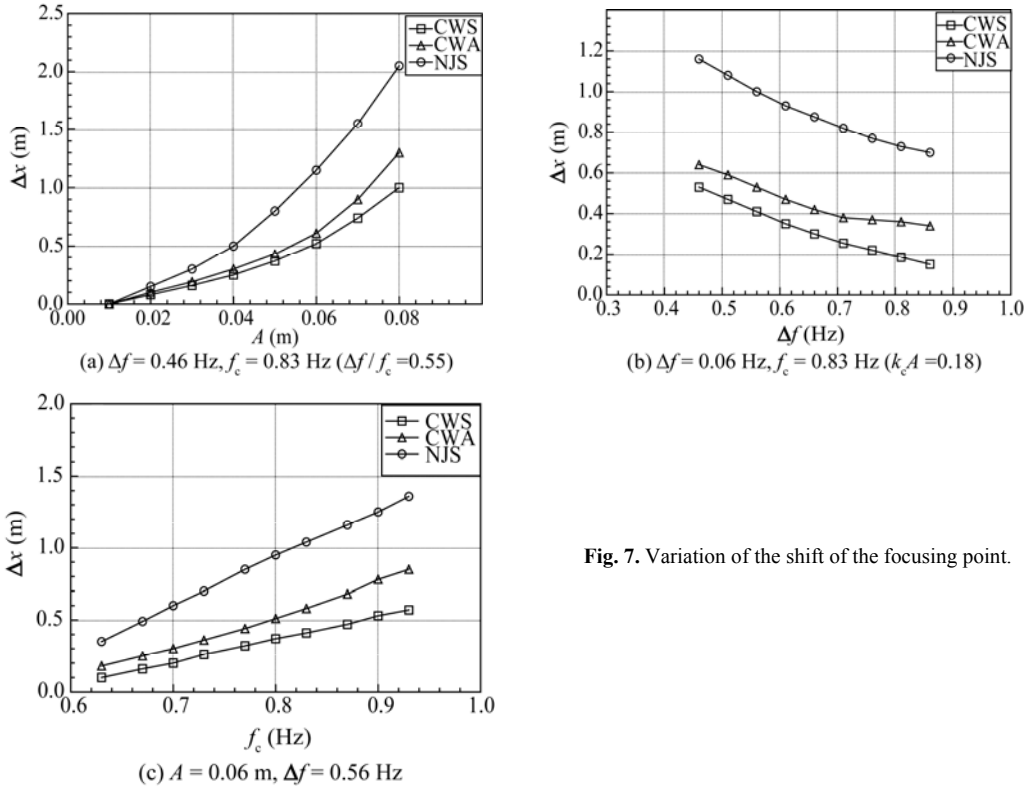

(a) Δf = 0.46 Hz, f_c = 0.83 Hz ($\Delta f / f_c$ =0.55)

(b) Δf = 0.06 Hz, f_c = 0.83 Hz ($k_c A$ =0.18)

(c) A = 0.06 m, Δf = 0.56 Hz

Fig. 7. Variation of the shift of the focusing point.

To illustrate the variation of the maximum crest with the wave parameters, Fig. 8 shows the results of the calculated maximum crest of the wave group for different wave parameters. Fig. 8a presents the relation between the calculated maximum crest and the assumed amplitude of the focused wave for different amplitude distributions. It can be seen that the maximum crest becomes larger as the assumed focused amplitude increases, and the difference between the calculated results and the linear results also become larger. This is reasonable, because the nonlinear interaction becomes stronger as the focused amplitude increases. In Fig. 8b, the maximum crest of the wave group with the CWS distribution decreases slightly as the frequency bandwidth increases, whereas there is nearly no change for waves with the CWA or NJS distribution. In Fig. 8c, the maximum crest increases as the central frequency increases. This is attributed to strong nonlinear interactions within the wave group for a high central frequency.

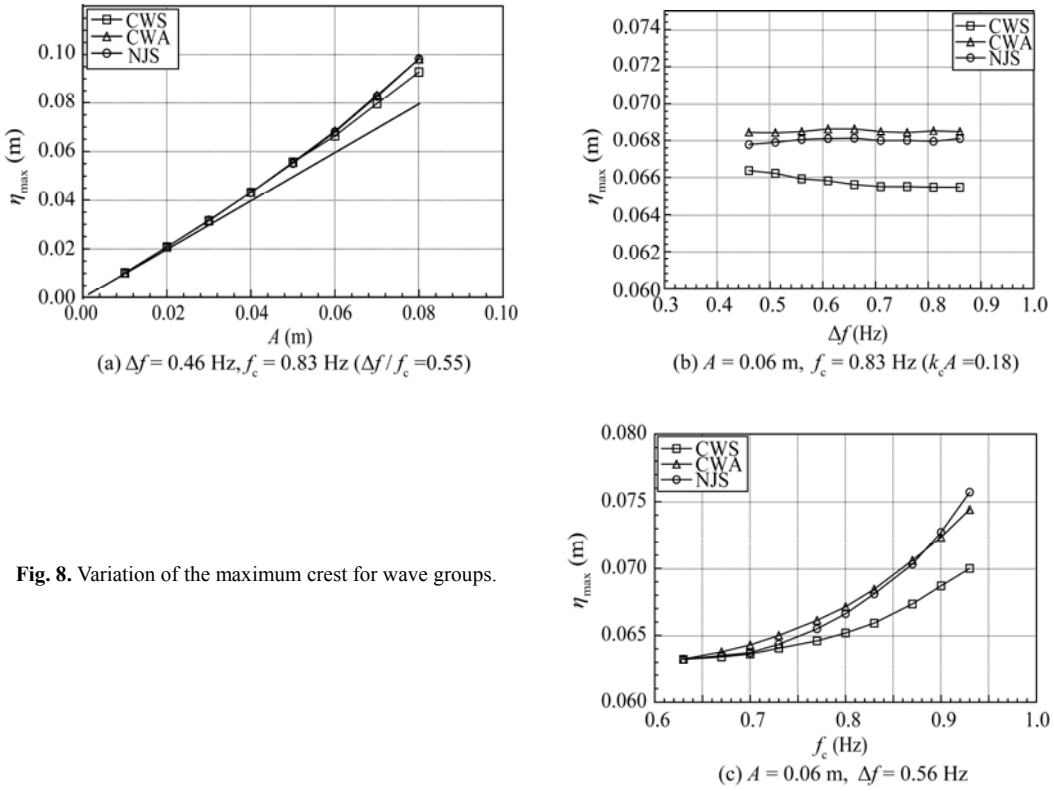

Fig. 8. Variation of the maximum crest for wave groups.

5.2 Three-Dimensional Focused Waves

In a real sea, waves are multidirectional. In order to investigate the effects of wave directionality on the properties of focused waves, directional focused waves with different spreading parameters s were numerically simulated. The assumed amplitude of the focused waves was 0.08 m, the frequency bandwidth was in the range of 0.60–1.06 Hz and the central frequency was 0.83 Hz. The CWA and CWS distributions were considered. θ_{max} was 60° and the directional spreading parameter s had values of 4, 6, 10, 20, 40 and 70. The area of the basin in the simulation was $L_x \times L_y$ = 20 m×28 m and the assumed focusing position was at (x, y)=(8.0, 14.0) m. The water depth was 3 m. In all simulation,

201×281 modes were used on the free surface, 281×64 on the wave maker boundary and order M=4.

Fig. 9 shows the variation of the maximum wave crest with the directional spreading parameter s for an assumed amplitude A=0.08 m. It can be seen that the maximum wave crest increases as s increases (directional spreading becomes narrower). This is because the strong nonlinear interaction between wave components for large values of s may occur and be consistent with the phenomenon observed in the experiments of She *et al*. (1994) that when the directional spreading was large, a large assumed amplitude needed to be input. Also, the generated wave amplitude for the CWA distribution is larger than that for the CWS distribution. This means that waves generated with the CWA distribution break more easily. Fig. 10 shows the relationship between the shift of the focusing point and the directional spreading concentration parameter s. For the same reason as in the case of the maximum crest, the shift of the focusing point increases as the directional spreading parameter increases. Similarly, the shift of the focusing point for the CWA distribution is larger than that for the CWS distribution. In other words, the large directional spreading reduces the nonlinear processes and reduces the differences of the calculated wave amplitude and the position of the focusing point from the assumed values. It also implies that when wave direction spreading is wide, the strong nonlinear interaction (third-order nonlinear) is weak.

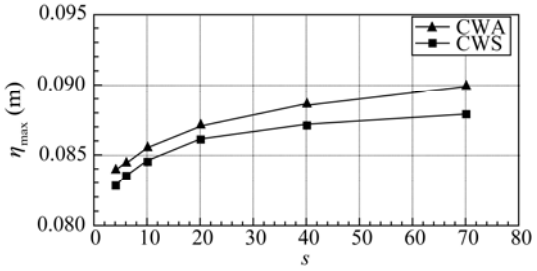

Fig. 9. Variation of the maximum wave crest of the wave group with the directional spreading concentration parameter.

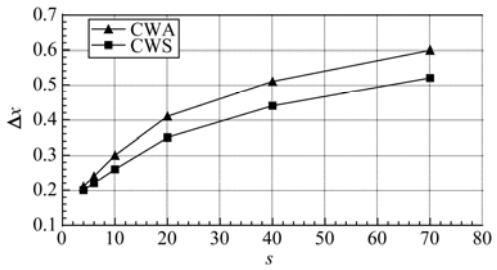

Fig. 10. Variation of the shift of the focusing point with the directional spreading concentration parameter.

Field and laboratory studies have shown that, during the process of nonlinear wave propagation, both horizontal and vertical asymmetries of the wave surface occur, and thus the profile deviates from the symmetric profile of the theoretical wave shape (Kjeldsen and Myrhaug, 1980; Tulin and Li, 1991). In order to investigate the effects of wave directionality on the properties of the wave surface, five wave surface parameters are considered, namely:

- the crest front steepness $\varepsilon = 2\pi\eta_{max}/(gT_1T)$;
- the crest rear steepness $\delta = 2\pi\eta_{max}/(gT_2T)$;
- the total steepness $\varepsilon_T = 2\pi\eta_{max}/(gT^2)$;
- the vertical asymmetry factor $\lambda = T_2/T_1$;
- the horizontal asymmetry factor $\mu = \eta_{max}/H$.

The quantities involved in the definitions of these wave surface parameters are shown in Fig. 11. These parameters can be used to characterize steep or breaking waves. Following Kjeldsen and Myrhaug (1980), these parameters were estimated from temporal records of the surface displacement using zero-down cross analysis.

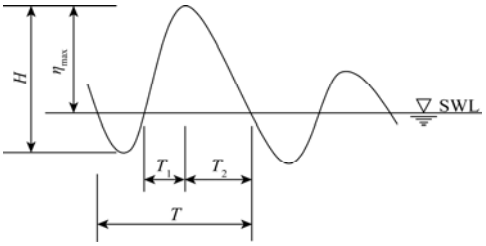

Fig. 11. Definition of the parameters used in the calculation of wave surface parameters.

Figs. 12 and 13 show the variation of these wave surface parameters along the centreline for multidirectional focused waves with different directional spreading concentration parameters for the CWA and CWS distributions. It can be seen that when the directional spreading is narrower (i.e., the directional spreading concentration parameter s is larger), as the waves are focused at the focusing point, the crest front steepness, the crest rear steepness, and the total wave steepness increase. At the focusing point, these parameters reach their maximum values. After the waves have propagated past the focusing point, the parameters decrease. From Figs. 12c and 13c, we can see that when s becomes larger, which means that the directional spreading is narrower, the crest front steepness, the crest rear steepness, and the total wave steepness increase rapidly. It can be imagined that the waves may break before the focusing point if the wave front is steep enough. At the same time, the vertical asymmetry factor λ changes rapidly during the propagation and the horizontal asymmetry factor μ is much larger than 0.5. This means that the wave surface is not symmetrical in the horizontal and vertical directions and the crests are always larger than the troughs. Also, the variation of the vertical and horizontal asymmetry factors depends on the directional spreading parameter s. The variation as s increases is fast.

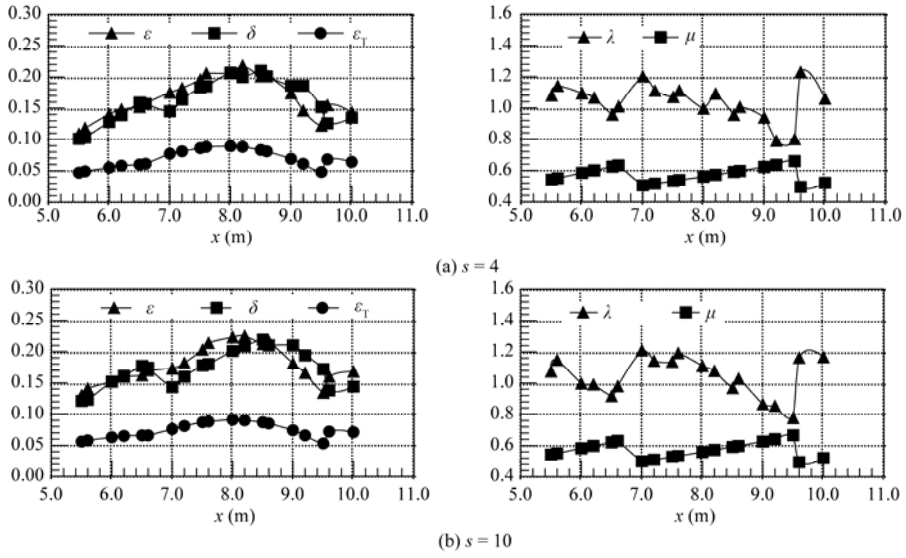

Fig. 12. Wave surface parameters along the centreline for different directional spreading concentration parameters in the case of the CWA distribution (to be continued).

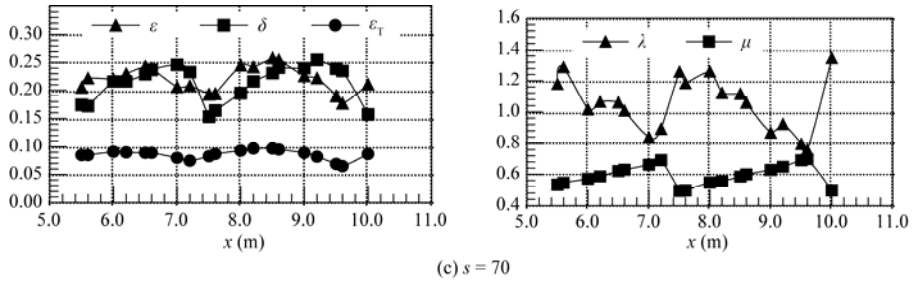

(c) $s = 70$

Fig. 12. (continued) Wave surface parameters along the centreline for different directional spreading concentration parameters in the case of the CWA distribution.

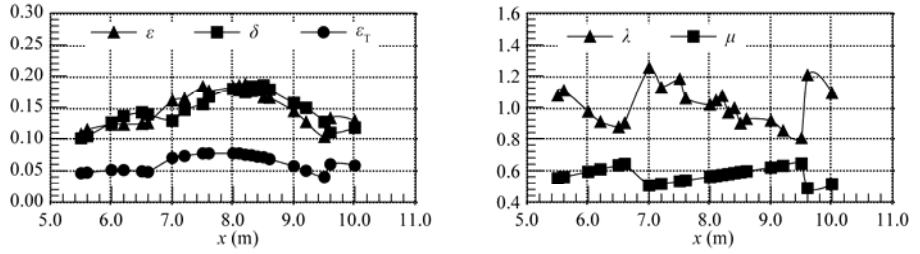

(a) $s = 4$

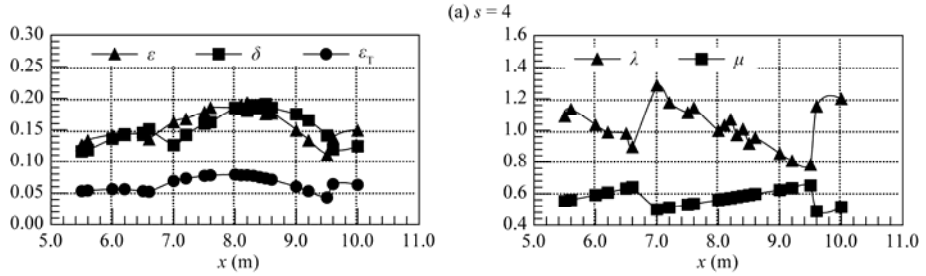

(b) $s = 10$

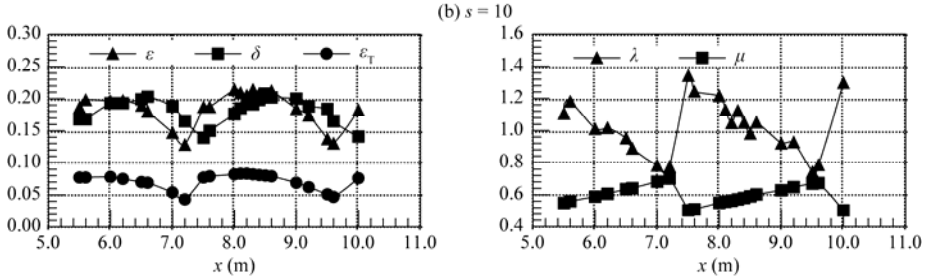

(c) $s = 70$

Fig. 13. Wave surface parameters along the centreline for different directional spreading concentration parameters in the case of the CWS distribution.

To further show the effect of wave directionality on wave surface parameters, Fig. 14 shows the variation of wave surface parameters at the focusing point with the directional concentration parameter s. It can be seen that the surface parameters increase as s increases. In other words, the wave directionality can increase the wave surface parameters and therefore affect the breaking criterion. This is consistent with the results of previous experimental studies by She *et al*. (1994) and may be the cause of the very scattered parameters observed for waves in the field.

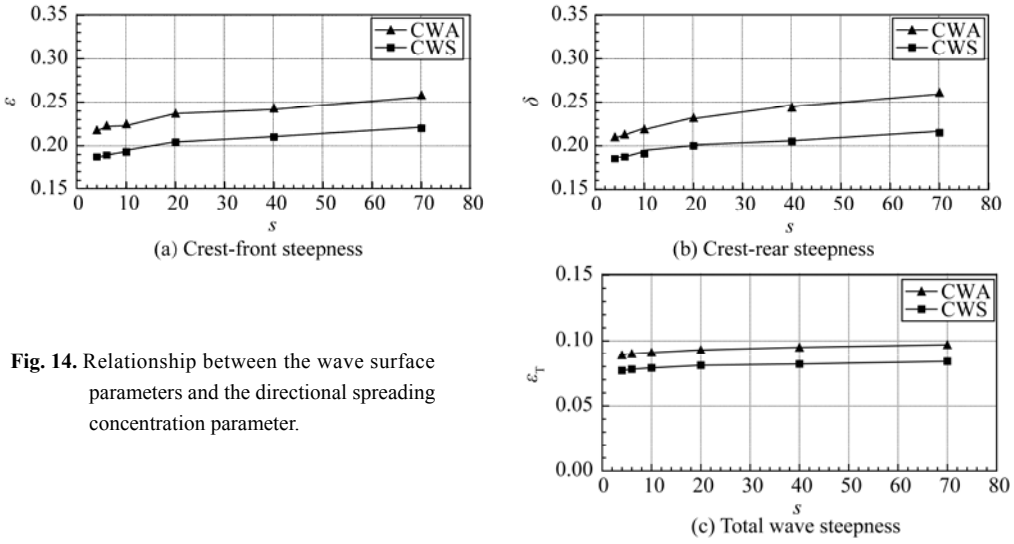

Fig. 14. Relationship between the wave surface parameters and the directional spreading concentration parameter.

6. Conclusions

In this paper, a numerical model based on a high order spectral formulation is described in which a wave maker boundary is introduced. This model can be used to simulate the focusing of three-dimensional waves. The properties of two-dimensional and three-dimensional focused waves are investigated using the numerical model.

The effects of the wave parameters on the two-dimensional surface elevation, including the shift of the focusing point and the maximum crest, are discussed. The obtained results show that the shift of the focusing point and the maximum crest of the wave group increase as the assumed amplitude of the focused wave and the central frequency increase. This is attributed to the stronger nonlinear interaction for a larger wave steepness. They imply that the strong nonlinear interaction has influence on wave focusing. The characteristics of the wave are also evidently dependent on the wave amplitude distribution and the frequency bandwidth.

For the three-dimensional focused waves, the maximum wave crest and the shift of the focusing point decrease as the directional spreading parameter decreases and the directional spreading increases. This means that a broad directional spreading weakens the strong nonlinear interactions between the wave components. The relations between the wave surface parameters and the directional spreading also illustrate this phenomenon. Conversely, the wave directionality can increase the wave surface parameters and affect the breaking criterion.

References

Agnon, Y. and Bingham, H. B., 1999. A non-periodic spectral method with application to nonlinear water waves, *Eur. J. Mech. B/Fluids*, **18**(3): 527–534.

Baldock, T. E., 1994. *Nonlinear Transient Water Waves*, Ph. D. Thesis, Imperial College of Science, Technology and Medicine, United Kingdom.

Baldock, T. E., Swan, C. and Taylor, P. H., 1996. A laboratory study of nonlinear surface waves on water, *Phil.*

Trans. Roy. Soc. Lond., *Ser. A*, **354**(1707): 649–676.

Bonnefoy, F., Ducrozet, G., Le Touzé, D. and Ferrant, P., 2009. Time domain simulation of nonlinear water waves using spectral methods, *Advances in Numerical Simulation of Nonlinear Water Waves*, **11**, 129–164.

Bonnefoy, F., Le Touzé, D. and Ferrant, P., 2004. Generation of fully-nonlinear prescribed wave fields using a high-order spectral model, *Proc. 14th Int. Offshore Polar Eng. Conf*., Toulon, France, **3**, 257–263.

Brandini, C. and Grilli, S., 2001. Modeling of freak wave generation in a 3D NWT, *Proc. 11th Int. Offshore Polar Eng. Conf.*, Stavanger, Norway, **3**, 124–131.

Dean, R. G. and Dalrymple, R. A., 1984. *Water Wave Mechanics for Engineers and Scientists*, Prentice-hall Inc.

Dommermuth, D. G. and Yue, D. K. P., 1987. A high-order spectral method for the study of nonlinear gravity waves, *J. Fluid Mech.*, **184**, 267–288.

Ducrozet, G., Bonnefoy, F, Le Touzé, D. and Ferrant, P., 2012. A modified high-order spectral method for wavemaker modeling in a numerical wave tank, *Eur. J. Mech. B/Fluids*, **34**, 19–34.

Goda, Y., 1999. A comparative review on the functional forms of directional wave spectrum, *Coast. Eng. J.*, **41**(1): 1–20.

Johannessen, T. B. and Swan, C., 2001. A laboratory study of the focusing of transient and directionally spread surface water waves, *Proc. Roy. Soc. Lond.*, *Ser. A*, **457**(2008): 971–1006.

Kharif, C. and Pelinovsky, E., 2003. Physical mechanisms of the rogue wave phenomenon, *Eur. J. Mech. B/Fluids*, **22**(6): 603–634.

Kjeldsen, S. P. and Myrhaug, D., 1980. Wave-wave interactions, current-wave interactions and resulting extreme waves and breaking waves, *Proceedings of 17th Conference on Coastal Engineering*, Sydney, Australia, 2277–2303.

Larsen, J. and Dancy, H., 1983. Open boundaries in short wave simulation-a new approach, *Coast. Eng.*, **7**(3): 285–291.

Li, J. X., Liu, S. X. and Hong, K., 2008. Numerical study of two-dimensional focusing waves, *China Ocean Eng.*, **22**(2): 253–266.

Liu, S. X. and Hong, K. Y., 2005. Physical investigation of directional wave focusing and breaking waves in wave basin, *China Ocean Eng.*, **19**(1): 21–35.

Rapp, R. J. and Melville, W. K., 1990. Laboratory measurements of deep-water breaking waves, *Phil. Trans. Roy. Soc. Lond. Ser. A*, **331**(1622): 735–800.

Sharma, J. N. and Dean, R. G., 1981. Second-order directional seas and associated wave forces, *Society of Petroleum Engineers Journal*, **4**, 129–140.

She, K., Created, C. A. and Easson, W. J., 1994. Experimental study of three-dimensional breaking wave, *J. Waterw. Port Coast. Ocean Eng.,* ASCE, **120**(1): 20–36.

Tulin, M. P. and Li, J. J., 1991. On the breaking of energetic waves, *Proc. 1st Int. Offshore Polar Eng. Conf.*, Edinburgh, UK, 498–503.

West, B. J., Brueckner, K. A., Janda, R. S., Milder, D. M. and Milton, R. L., 1987. A new numerical method for surface hydrodynamics. *J. Geophys. Res.*, **92**(C11): 11803–11824.

Wu, C. H. and Nepf, H. M., 2002. Breaking criteria and energy losses for three-dimensional wave breaking, *J. Geophys. Res*., **107**(C10): 3177, doi:10.1029/2001JC001077.

Zakharov, V. E., 1968. Stability of periodic waves of finite amplitude on the surface of a deep fluid, *J. Appl. Mech. Tech. Phys.*, **9**(2): 190–194.